



## Abstract

Measuring water vapor in the upper troposphere and lower stratosphere is difficult due to the low mixing ratios found there, typically only a few parts per million. Here we examine near infrared spectra acquired with the Solar Spectral Flux Radiometer during the first science phase of the NASA Airborne Tropical Tropopause EXperiment. From the 1400 and 1900 nm absorption bands, we infer water vapor amounts in the tropical tropopause layer and adjacent regions between 14 and 18 km altitude. We compare these measurements to solar transmittance spectra produced with the MODerate resolution atmospheric TRANsmission (MODTRAN) radiative transfer model, using in situ water vapor, temperature, and pressure profiles acquired concurrently with the SSFR spectra. Measured and modeled transmittance values agree within 0.002, with some larger differences in the 1900 nm band (up to 0.004). Integrated water vapor amounts along the absorption path lengths of 3 to 6 km varied from  $1.26 \times 10^{-4}$  to  $4.59 \times 10^{-4} \text{ g cm}^{-2}$ . A 0.002 difference in absorptance at 1367 nm results in a  $3.35 \times 10^{-5} \text{ g cm}^{-2}$  change of integrated water vapor amount, 0.004 absorptance change at 1870 nm results in  $5.5 \times 10^{-5} \text{ g cm}^{-2}$  of water vapor. These are 27 % (1367 nm) and 44 % (1870 nm) differences at the lowest measured value of water vapor ( $1.26 \times 10^{-4} \text{ g cm}^{-2}$ ) and 7 % (1367 nm) and 12 % (1870 nm) differences at the highest measured value of water vapor ( $4.59 \times 10^{-4} \text{ g cm}^{-2}$ ). A potential method for extending this type of measurement from aircraft flight altitude to the top of the atmosphere (TOA) is discussed.

## 1 Introduction

Water vapor in the stratosphere has important climatic (Forster and Shine, 2002; Solomon et al., 2010), dynamical (Joshi et al., 2006; Maycock et al., 2013), and chemical impacts (Stenke and Grewe, 2005). The long-term trends in water vapor have shown a general increase over the period of reliable measurements, starting in the

## UT and LS water vapor retrievals from the 1400 and 1900 nm water vapor bands

B. C. Kindel et al.

Title Page

Abstract

Introduction

Conclusions

References

Tables

Figures



Back

Close

Full Screen / Esc

Printer-friendly Version

Interactive Discussion



## UT and LS water vapor retrievals from the 1400 and 1900 nm water vapor bands

B. C. Kindel et al.

Title Page

Abstract

Introduction

Conclusions

References

Tables

Figures



Back

Close

Full Screen / Esc

Printer-friendly Version

Interactive Discussion



1970s with balloon borne hygrometer measurements (Oltmans et al., 2000; Rosenlof et al., 2001; Hurst et al., 2011). Later satellite measurements from, for example, the Halogen Occultation Experiment (HALOE), extended these measurements to global scales from the geographically limited balloon measurements (e.g. Remsberg et al., 1996; Dessler and Kim, 1999). The record of stratospheric water vapor since 2000 has shown periods of both increasing and decreasing concentrations (Randel et al., 2004; Scherer et al., 2008; Fueglistaler, 2012; Nedoluha et al., 2013). The mechanisms driving changes in stratospheric water vapor concentrations are currently unresolved.

The transport of air from the troposphere to the stratosphere occurs mainly in the tropics (Brewer, 1949). Water vapor moving from the tropical troposphere to the stratosphere must pass through the so-called tropical tropopause layer (TTL) (Fueglistaler et al., 2009), characterized by very low temperatures. The TTL acts as a cold trap, “freeze drying” air as it passes through, limiting the entry of water vapor into the stratosphere (Brewer, 1949). Understanding the fate of water vapor as it encounters the TTL is one of the main science objectives of the NASA Airborne Tropical Tropopause Experiment (ATTREX).

The first ATTREX science flights were conducted on the NASA Global Hawk (GH) aircraft from NASA Dryden Flight Research Center at Edwards Air Force Base in southern California during February and March of 2013. The GH carried instruments that measured atmospheric state, composition, and radiation. Included in these were measurements of downwelling solar spectral irradiance, in situ water vapor mixing ratio, pressure, and temperature. In this work we examine the use of strong water vapor absorption bands in the near infrared (NIR) spectrum to infer water vapor amounts across the TTL, in the upper troposphere and lower stratosphere (UT/LS). Observed NIR water vapor absorptances are compared to model predicted absorptances using in situ profiles of water vapor, pressure, and temperature as input to the atmospheric radiative transfer model MODTRAN5 version 5.3.2 (Berk et al., 2006).

In addition to the sensitivity to even very small amounts of water vapor, these bands have the additional benefit of being virtually free of molecular (Rayleigh) scattering and







From these profiles, those performed during daylight (11 total during the experiment period) were selected for analysis. Figure 3 shows the first two profiles from the first science flight on 2 February 2013.

The derivation of atmospheric transmittance from the vertical profiles of solar spectral irradiance was straightforward. Five to ten minutes (300–600 spectra) of zenith SSFR data immediately prior to and after the descent from 18 km were averaged to give a robust measurement of the downward spectral irradiance at this altitude. The averaging both increases the SNR of the measurement and reduces the effects of altitude (pitch and roll) changes that are unavoidable during flight. The same averaging was performed during the period of level flight at the bottom of the profile near 14 km. These time periods are over-plotted in red ( $\sim 18$  km) and blue ( $\sim 14$  km) in Fig. 3. Transmittance spectra ( $T$ ) were created from these averaged spectra by dividing the low altitude average zenith downwelling irradiance ( $F_{14\text{km}}$ ) by the high altitude average zenith downwelling irradiance at ( $F_{18\text{km}}$ ):

$$T = \frac{F_{14\text{km}}}{F_{18\text{km}}} \quad (1)$$

The total absorption path length, denoted with the letter  $H$  in the Fig. 6 depends on the altitude change of the aircraft profile ( $\Delta Z$ ) and the solar zenith angle (SZA) during the profile;  $H$  increases with increasing SZA. The vertical profiles during ATTREX were 3–4 km in  $Z$ ; the range of solar zenith angles during the profiles produced values for  $H$  up to 5.93 km.

Figure 4 shows the resultant measured transmittance spectra from the first two profiles. The water vapor bands are shaded in gray, the  $\text{CO}_2$  bands in green, and the oxygen band in red.  $\text{CO}_2$  and  $\text{O}_2$  absorption features in the near infrared are of little interest to this work other than to note their presence in the spectra. Figure 5 shows the NW measurement of the water vapor number density and integrated  $\text{H}_2\text{O}$  amount over the vertical profile. The measured integrated water vapor for the second profile was approximately three times greater (Fig. 5, right hand panel) than the first profile (Fig. 5

## UT and LS water vapor retrievals from the 1400 and 1900 nm water vapor bands

B. C. Kindel et al.

[Title Page](#)[Abstract](#)[Introduction](#)[Conclusions](#)[References](#)[Tables](#)[Figures](#)[Back](#)[Close](#)[Full Screen / Esc](#)[Printer-friendly Version](#)[Interactive Discussion](#)

left hand panel). In Fig. 4 the differences in the integrated water vapor paths are clearly indicated in the transmittances derived from the SSFR irradiances. The second profile, with the higher water vapor amount had a significantly lower relative transmittance in the water vapor bands than the first profile.

## 5 Radiative transfer modeling

To assess the ability of SSFR measurements to infer water vapor across these relatively small absorption path lengths (3–6 km) and small water vapor amounts, radiative transfer modeling of the vertical profile transmittance was performed for comparison with the measured transmittances. The atmospheric radiative transfer model, MODTRAN5, was run using the profiles of water vapor concentration from the NW instrument and the profiles of temperature and pressure from MMS as input. MODTRAN5 was used to calculate the solar spectral irradiance at the altitudes of the top and bottom of each GH profile. The ratio of the two yields the transmittance spectrum in an identical manner to the SSFR measurements (Eq. 1).

MODTRAN5 uses a correlated-k model for gaseous absorption (Lacis et al., 1991). This MODTRAN version of the band model includes updated line parameters from the HITRAN 2008 line database (Rothman et al., 2009). The water vapor continuum is modeled using the Clough–Kneizys Water Vapor Continuum version 2.4. (Mlawer et al., 2012). The CO<sub>2</sub> mixing ratios were set to 392 ppmv.

The MODTRAN5 atmospheric profiles over the range of the GH profiles were modified to include the measurements of water vapor from NW and pressure and temperature from MMS. Altitudes above and below the aircraft flight level were set to the default tropical profile values. Over the range of the aircraft profile, the model atmospheric levels were set to every 250 m resulting in about 12 levels for each profile. The water vapor number densities were linearly interpolated to the model levels (e.g., 14.250, 14.500, 14.750 km. . .) and were scaled to ensure that the integrated water vapor amount in the model (lower vertical resolution) matched that of the integrated NW measurements

### UT and LS water vapor retrievals from the 1400 and 1900 nm water vapor bands

B. C. Kindel et al.

Title Page

Abstract

Introduction

Conclusions

References

Tables

Figures



Back

Close

Full Screen / Esc

Printer-friendly Version

Interactive Discussion



(higher vertical resolution). The downwelling spectral irradiance was calculated for the mean of the high altitude and low altitude legs of the GH profile and the ratio of the two resulted in the atmospheric transmittance over the absorption path length.

To estimate the effects of the water vapor variability on the calculated transmittance spectra, water vapor measurement variation was propagated into the model by including plus and minus one standard deviation of NW water vapor number densities in the model profiles. The model was run at  $1\text{ cm}^{-1}$  sampling and  $2\text{ cm}^{-1}$  resolution. Computed spectra were convolved with the slit function of the SSFR for direct comparison with the measurements.

## 6 Results

In Figs. 6–8 the measured and modeled transmittance spectra for all eleven profiles included in this study are plotted. The individual profiles are labeled SF (Science Flight) followed by the science flight number and the profile number. For example, SF-2-2 corresponds to science flight number two (9 February 2013) and the second profile during that flight. There were two daylight profiles per flight with the exception of the third flight, which had only one profile.

The mean SSFR spectra are plotted in black and the model spectra in blue. The modeled spectra at plus/minus one standard deviation of measured water vapor are shown in red. In general, the spatial variation in the water vapor profiles has little effect on the computed transmittance spectra, 0.001 or less, and indeed it is difficult to distinguish the mean spectra in blue from the standard deviation spectra in red in most of the plots.

The right-hand columns in Figs. 6–8 show the measured-modeled residual spectra. In general, measured and modeled transmittances agree to within 0.002 in the 1400 nm water band and 0.003 to 0.004 in the 1900 nm band. Figure 9 shows the mean and standard deviation difference spectrum for the eleven cases. The MODTRAN5 computed absorptance is slightly greater than that measured by SSFR in both the 1400

### UT and LS water vapor retrievals from the 1400 and 1900 nm water vapor bands

B. C. Kindel et al.

Title Page

Abstract

Introduction

Conclusions

References

Tables

Figures



Back

Close

Full Screen / Esc

Printer-friendly Version

Interactive Discussion







**UT and LS water vapor retrievals from the 1400 and 1900 nm water vapor bands**

B. C. Kindel et al.

Title Page

Abstract

Introduction

Conclusions

References

Tables

Figures

◀

▶

◀

▶

Back

Close

Full Screen / Esc

Printer-friendly Version

Interactive Discussion



The intercepts of these equations are very near zero ( $\sim 10^{-6}$ ) as expected; zero absorptance should correspond to zero water vapor amount. These linear fits provide a simple method for estimating the uncertainty of the SSFR absorptance measurement in terms of water vapor amount. For instance, an uncertainty of 0.002 in the SSFR absorptance at 1367 nm (the mean difference between the model and the measurements) corresponds to a  $3.35 \times 10^{-5} \text{ g cm}^{-2}$  integrated water vapor change. Similarly, a 0.004 change in absorptance at 1870 nm results in a  $5.51 \times 10^{-5} \text{ g cm}^{-2}$  change in water vapor amount.

In practice, a model TOA spectrum would be fit at these wavelengths to a SSFR spectrum and the ratio calculated. A pre-calculated lookup table of absorptances generated from a range of water vapor amounts, solar zenith angles, and altitudes would be used to determine the integrated water vapor amount above the aircraft. This retrieval could be undertaken in near real-time from aircraft equipped with high bandwidth downlinks. This type of real-time retrieval is becoming more common with the introduction of such satellite downlinks to the NASA ER-2 and Global Hawk aircraft. In the lower left panel of Fig. 11, the water vapor amounts corresponding to the transmittances are plotted as a function of altitude. The values for the transmittances plotted in the top left panel are color-coded. The range of water vapor amounts fall within the same range as those measured in the UT/LS during ATTREX, indicating that stratospheric water vapor amounts are within the capability of the SSFR to measure. However, this will require that radiometric calibration of the instrument be modified to remove the water vapor surrounding the laboratory setup. The water vapor bands can have significant (1–2 % absorption) even over the path length (50 cm) from the NIST irradiance standard to the light collector (Kindel et al., 2001). The absorption by water vapor in the laboratory radiometric calibration of the SSFR has likely masked the small absorption in previous SSFR measurements.

## 8 Summary and conclusions

Water vapor in the upper atmosphere has important climatic, dynamical and chemical impacts on the Earth's atmosphere. The accurate measurement of water vapor in the upper troposphere and stratosphere is important in quantifying these impacts. In this work we have examined the use of the strong water vapor bands in the solar spectrum to infer water vapor amount in the UT/LS. This work, unlike most previous work using solar transmittance type retrievals, used aircraft in situ measurements of water vapor vertical profiles over very small mixing ratios, a few ppmv, to predict the transmittance and compare with measurements. Most solar transmittance type retrievals have little if any independent validation of water vapor amount, vertical distribution, pressure, or temperature profile (Schwab et al., 1996; Harries et al., 1996).

Comparisons of modeled and measured transmittance spectra for eleven cases resulted in spectra that agreed to generally 0.002 in transmittance with deviations up to 0.004 in some channels of the 1900 nm band. The measurement uncertainty is approximately 0.001 as demonstrated by the repeatability of the measurements in non-absorbing wavelengths (e.g. 1300 nm). This increases to 0.002 at longer wavelengths where the SNR is not as high.

A technique for inferring water vapor from zenith viewing aircraft solar spectral irradiance has been outlined. This technique relies on the use of wavelengths surrounding the strong NIR water vapor bands where the atmosphere is essentially transparent. Radiative transfer modeling of water vapor transmittance from altitudes of 14 to 20 km, indicate that integrated water vapor amounts, and thus the transmittances from these altitudes to the TOA fall in a similar range to the shorter path lengths examined in this work. This technique could potentially produce near real-time retrievals of aircraft to the TOA water vapor amounts. Work is required to modify the radiometric calibration to remove the effects of water vapor in the laboratory as well as forward radiative transfer modeling to determine the integrated water vapor amounts from the measurement of transmittance.

### UT and LS water vapor retrievals from the 1400 and 1900 nm water vapor bands

B. C. Kindel et al.

Title Page

Abstract

Introduction

Conclusions

References

Tables

Figures



Back

Close

Full Screen / Esc

Printer-friendly Version

Interactive Discussion



*Acknowledgements.* The authors wish to acknowledge the support of the SSFR instrument during ATTREX by Warren Gore and Tony Trias of NASA Ames Research Center. We also thank David Fahey of NOAA for his encouragement in investigating atmospheric water vapor with solar spectral irradiance during ATTREX. This work was supported by NASA award NNX10AO84A.

## References

- Berk, A., Anderson, G. P., Acharya, P. K., Bernstein, L. S., Muratov, L., Lee, J., Fox, M., Adler-Golden, S. M., Chetwynd, J. H., Hoke, M. L., Lockwood, R. B., Gardner, J. A., Cooley, T. W., Borel, C. C., Lewis, P. E., and Shettle, E. P.: MODTRAN5: 2006 Update, P. Soc. Photo-Opt. Ins., 6233, 62331F, doi:10.1117/12.665077, 2006.
- Brewer, A. W.: Evidence for a world circulation provided by the measurements of helium and water vapour distribution in the stratosphere, Q. J. Roy. Meteor. Soc., 75, 351–363, doi:10.1002/qj.49707532603, 1949.
- Chiou, E. W., McCormick, M. P., and Chu, W. P.: Global water vapor distributions in the stratosphere and upper troposphere derived from 5.5 years of SAGE II observations (1986–1991), J. Geophys. Res., 102, 19105–19118, doi:10.1029/97JD01371, 1997.
- Chu, W. P., Chiou, E. W., Larsen, J. C., Thomason, L. W., Rind, D., Buglia, J. J., Oltmans, S., McCormick, M. P., and McMaster, L. M.: Algorithms and sensitivity analyses for Stratospheric Aerosol and Gas Experiment II water vapor retrieval, J. Geophys. Res., 98, 4857–4866, doi:10.1029/92JD01628, 1993.
- Dessler, A. E. and Kim, H.: Determination of the amount of water vapor entering the stratosphere based on Halogen Occultation Experiment (HALOE) data, J. Geophys. Res., 104, 30605–30607, doi:10.1029/1999JD900912, 1999.
- Forster, P. M. and Shine, K. P.: Assessing the climatic impacts of trends in stratospheric water vapour, Geophys. Res. Lett., 29, 1086–1089, 2002.
- Fueglistaler, S., Dessler, A. E., Dunkerton, T. J., Folkins, I., Fu, Q., and Mote, P. W.: Tropical tropopause layer, Rev. Geophys., 47, RG1004, doi:10.1029/2008RG000267, 2009.
- Goody, R. M. and Yung, Y. L.: Atmospheric Radiation: Theoretical Basis, Oxford University Press, New York, 1989.

## UT and LS water vapor retrievals from the 1400 and 1900 nm water vapor bands

B. C. Kindel et al.

Title Page

Abstract

Introduction

Conclusions

References

Tables

Figures



Back

Close

Full Screen / Esc

Printer-friendly Version

Interactive Discussion



## UT and LS water vapor retrievals from the 1400 and 1900 nm water vapor bands

B. C. Kindel et al.

Title Page

Abstract

Introduction

Conclusions

References

Tables

Figures

◀

▶

◀

▶

Back

Close

Full Screen / Esc

Printer-friendly Version

Interactive Discussion



Harries, J. E., Russell III, J. M., Tuck, A. F., Gordley, L. L., Purcell, P., Stone, K., Bevilacqua, R. M., Gunson, M., Nedoluha, G., and Traub, W. A.: Validation of measurements of water vapor from the Halogen Occultation Experiment (HALOE), *J. Geophys. Res.*, 101, 10205–10216, doi:10.1029/95JD02933, 1996.

Hurst, D. F., Oltmans, S. J., Vömel, H., Rosenlof, K. H., Davis, S. M., Ray, E. A., Hall, E. G., and Jordan, A. F.: Stratospheric water vapor trends over Boulder, Colorado: analysis of the 30 year Boulder record, *J. Geophys. Res.*, 116, D02306, doi:10.1029/2010JD015065, 2011.

Joshi, M. M., Charlton, A. J., and Scaife, A. A.: On the influence of stratospheric water vapor changes on the tropospheric circulation, *Geophys. Res. Lett.*, 33, L09806, doi:10.1029/2006GL025983, 2006.

Kindel, B. C., Qu, Z., and Goetz, A. F. H.: Direct solar spectral irradiance and transmittance measurements from 350 to 2500 nm, *Appl. Optics*, 40, doi:10.1364/AO.40.003483, 2001.

Kurucz, R. L.: The solar irradiance by computation, in: *Proc. of the 17th Ann. Rev. Conf. on Atmos. Trans. Models*, edited by: Anderson, G. P., Picard, R. H., and Chetwynd, J. H., PL/TR-95-2060, Special Reports, No. 274, Pl. 332, Phillips Laboratory, Geophysics Directorate, MA, May 1995, 1995.

Lacis, A. A. and Oinas, V.: A description of the correlated  $k$  distribution method for modeling nongray gaseous absorption, thermal emission, and multiple scattering in vertically inhomogeneous atmospheres, *J. Geophys. Res.*, 96, 9027–9063, doi:10.1029/90JD01945, 1991.

Lucke, R. L., Korwan, D. R., Bevilacqua, R. M., Hornstein, J. S., Shettle, E. P., Chen, D. T., Daehler, M., Lumpe, J. D., Fromm, M. D., Debrestian, D., Neff, B., Squire, M., König-Langlo, G., and Davies, J.: The Polar Ozone and Aerosol Measurement (POAM) III instrument and early validation results, *J. Geophys. Res.*, 104, 18785–18799, doi:10.1029/1999JD900235, 1999.

Lumpe, J. D., Bevilacqua, R. M., Hoppel, K. W., and Randall, C. E.: POAM III retrieval algorithm and error analysis, *J. Geophys. Res.*, 107, 4575, doi:10.1029/2002JD002137, 2002.

Maycock, A. C., Joshi, M. M., Shine, K. P., and Scaife, A. A.: The circulation response to idealized changes in stratospheric water vapor, *J. Climate*, 26, 545–561, doi:10.1175/JCLI-D-12-00155.1, 2013.

Mlawer, E. J., Payne, V. H., Moncet, J.-L., Delamere, J. S., Alvarado, M. J., and Tobin, D. D.: Development and recent evaluation of the MT\_CKD model of continuum absorption, *Philos. T. R. Soc. A*, 370, 1–37, doi:10.1098/rsta.2011.0295, 2012.

## UT and LS water vapor retrievals from the 1400 and 1900 nm water vapor bands

B. C. Kindel et al.

Title Page

Abstract

Introduction

Conclusions

References

Tables

Figures



Back

Close

Full Screen / Esc

Printer-friendly Version

Interactive Discussion



Nedoluha, G. E., Michael Gomez, R., Allen, D. R., Lambert, A., Boone, C., and Stiller, G.: Variations in middle atmospheric water vapor from 2004 to 2013, *J. Geophys. Res.-Atmos.*, 118, 11285–11293, doi:10.1002/jgrd.50834, 2013.

Oltmans, S. J., Vömel, H., Hofmann, D. J., Rosenlof, K. H., and Kley, D.: The increase in stratospheric water vapor from balloon-borne, frost point hygrometer measurements at DC and Boulder, Colorado, *Geophys. Res. Lett.*, 27, 3453–3456, 2000.

Pilewskie, P., Pommier, J., Bergstrom, R. W., Gore, W., Howard, S., Rabette, M., Schmid, B., Hobbs, P. V., and Tsay, S. C.: Solar spectral radiative forcing during the Southern African Regional Science Initiative, *J. Geophys. Res.*, 108, 8486, doi:10.1029/2002JD002411, 2003.

Randel, W. J., Wu, F., Oltmans, S. J., Rosenlof, K., and Nedoluha, G. E.: Interannual changes of stratospheric water vapor and correlations with tropical tropopause temperatures, *J. Atmos. Sci.*, 61, 2133–2148, doi:10.1175/1520-0469(2004)061<2133:ICOSWV>2.0.CO;2, 2004.

Randel, W. J., Wu, F., Vömel, H., Nedoluha, G. E., and Forster, P.: Decreases in stratospheric water vapor after 2001: links to changes in the tropical tropopause and the Brewer–Dobson circulation, *J. Geophys. Res.*, 111, D12312, doi:10.1029/2005JD006744, 2006.

Remsberg, E. E., Bhatt, P. P., and Russell III, J. M.: Estimates of the water vapor budget of the stratosphere from UARS HALOE data, *J. Geophys. Res.*, 101, 6749–6766, doi:10.1029/95JD03858, 1996.

Rind, D., Chiou, E.-W., Chu, W., Oltmans, S., Lerner, J., Larsen, J., McCormick, M. P., and McMaster, L.: Overview of the Stratospheric Aerosol and Gas Experiment II water vapor observations: method, validation, and data characteristics, *J. Geophys. Res.*, 98, 4835–4856, doi:10.1029/92JD01174, 1993.

Rosenlof, K. H., Oltmans, S. J., Kley, D., Russell, J. M., Chiou, E.-W., Chu, W. P., Johnson, D. G., Kelly, K. K., Michelsen, H. A., Nedoluha, G. E., Remsberg, E. E., Toon, G. C., and McCormick, M. P.: Stratospheric water vapor increases over the past half-century, *Geophys. Res. Lett.*, 28, 1195–1198, doi:10.1029/2000GL012502, 2001.

Rothman, L. S., Gordon, I. E., Barbe, A., Benner, D. C., Bernath, P. F., Birk, M., Boudon, V., Brown, L. R., Campargue, A., Champion, J.-P., Chance, K., Coudert, L. H., Dana, V., Devi, V. M., Fally, S., Flaud, J.-M., Gamache, R. R., Goldman, A., Jacquemart, D., Kleiner, I., Lacombe, N., Lafferty, W., Mandin, J.-Y., Massie, S. T., Mikhailenko, S. N., Miller, C. E., Moazzen-Ahmadi, N., Naumenko, O. V., Nikitin, A. V., Orphal, J., Perevalov, V. I., Perrin, A., Predoi-Cross, A., Rinsland, C. P., Rotger, M., Simeckova, M., Smith, M. A. H., Sung, K., Tashkun, S. A., Tennyson, J., Toth, R. A., Vandaele, A. C., and Vander Auwera, J.: The HI-

**UT and LS water vapor retrievals from the 1400 and 1900 nm water vapor bands**

B. C. Kindel et al.

[Title Page](#)[Abstract](#)[Introduction](#)[Conclusions](#)[References](#)[Tables](#)[Figures](#)[Back](#)[Close](#)[Full Screen / Esc](#)[Printer-friendly Version](#)[Interactive Discussion](#)

TRAN 2008 molecular spectroscopic database, *J. Quant. Spectrosc. Ra.*, 110, 533–572, 2009.

Scherer, M., Vömel, H., Fueglistaler, S., Oltmans, S. J., and Staehelin, J.: Trends and variability of midlatitude stratospheric water vapour deduced from the re-evaluated Boulder balloon series and HALOE, *Atmos. Chem. Phys.*, 8, 1391–1402, doi:10.5194/acp-8-1391-2008, 2008.

Schwab, J. J., Pan, R.-J., and Zhang, J.: What constitutes a valid intercomparison of satellite and in situ stratospheric H<sub>2</sub>O measurements?, *J. Geophys. Res.*, 101, 1517–1528, doi:10.1029/95JD02999, 1996.

Solomon, S., Rosenlof, K. H., Portmann, R., Daniel, J., Davis, S., Sanford, T., and Plattner, G.-K.: Contribution of stratospheric water vapor changes to decadal variation in the rate of global warming, *Science*, 327, 1219–1222, 2010.

Stenke, A. and Grewe, V.: Simulation of stratospheric water vapor trends: impact on stratospheric ozone chemistry, *Atmos. Chem. Phys.*, 5, 1257–1272, doi:10.5194/acp-5-1257-2005, 2005.

Taha, G., Thomason, L. W., and Burton, S. P.: Comparison of Stratospheric Aerosol and Gas Experiment (SAGE) II version 6.2 water vapor with balloon-borne and space-based instruments, *J. Geophys. Res.*, 109, D18313, doi:10.1029/2004JD004859, 2004.

Thomason, L. W., Burton, S. P., Iyer, N., Zawodny, J. M., and Anderson, J.: A revised water vapor product for the Stratospheric Aerosol and Gas Experiment (SAGE) II version 6.2 data set, *J. Geophys. Res.*, 109, D06312, doi:10.1029/2003JD004465, 2004.



## UT and LS water vapor retrievals from the 1400 and 1900 nm water vapor bands

B. C. Kindel et al.

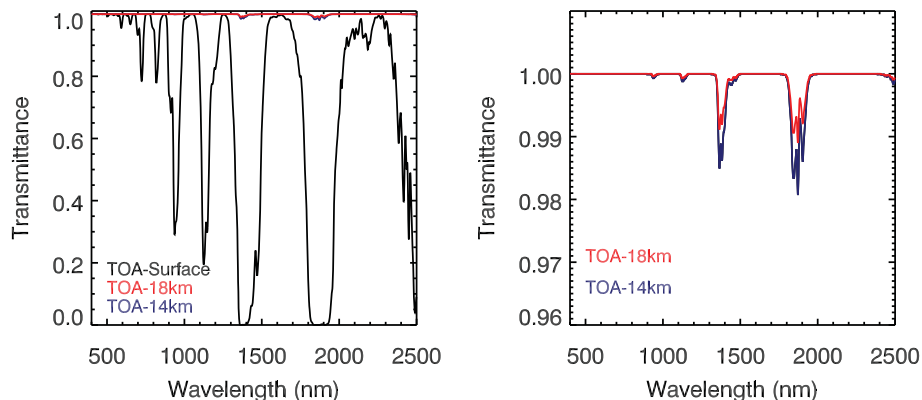


**Figure 2.** (left) Water vapor transmittance in a tropical atmosphere is shown from the surface (black), 14 km (blue) and 18 km (red) to the top of the atmosphere. (right) An expanded plot of the water vapor absorption high in the atmosphere at 1400 and 1900 nm.

Title Page

Abstract

Introduction

Conclusions

References

Tables

Figures

◀

▶

◀

▶

Back

Close

Full Screen / Esc

Printer-friendly Version

Interactive Discussion



## AMTD

7, 10221–10248, 2014

## UT and LS water vapor retrievals from the 1400 and 1900 nm water vapor bands

B. C. Kindel et al.

Title Page

Abstract

Introduction

Conclusions

References

Tables

Figures

◀

▶

◀

▶

Back

Close

Full Screen / Esc

Printer-friendly Version

Interactive Discussion

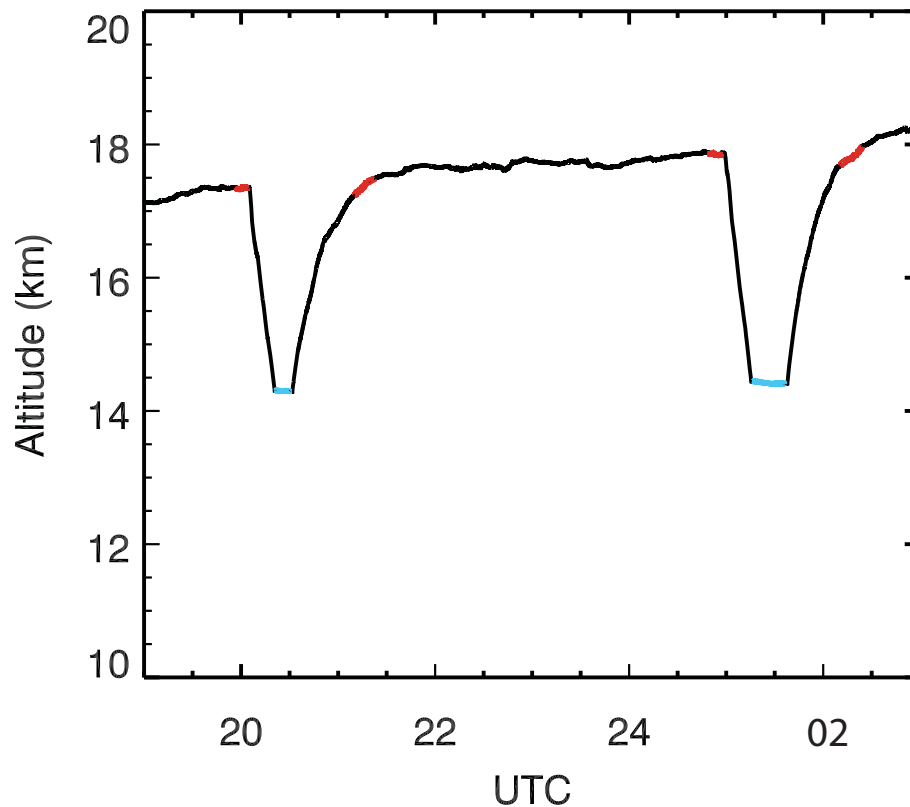


**Figure 3.** Two vertical profiles from the ATTREX science flight on 2 February 2013 are shown. The SSFR transmittances are created using ratios of data averaged from right before and after the profile (red) and during level flight at the lowest altitude (blue).

## UT and LS water vapor retrievals from the 1400 and 1900 nm water vapor bands

B. C. Kindel et al.

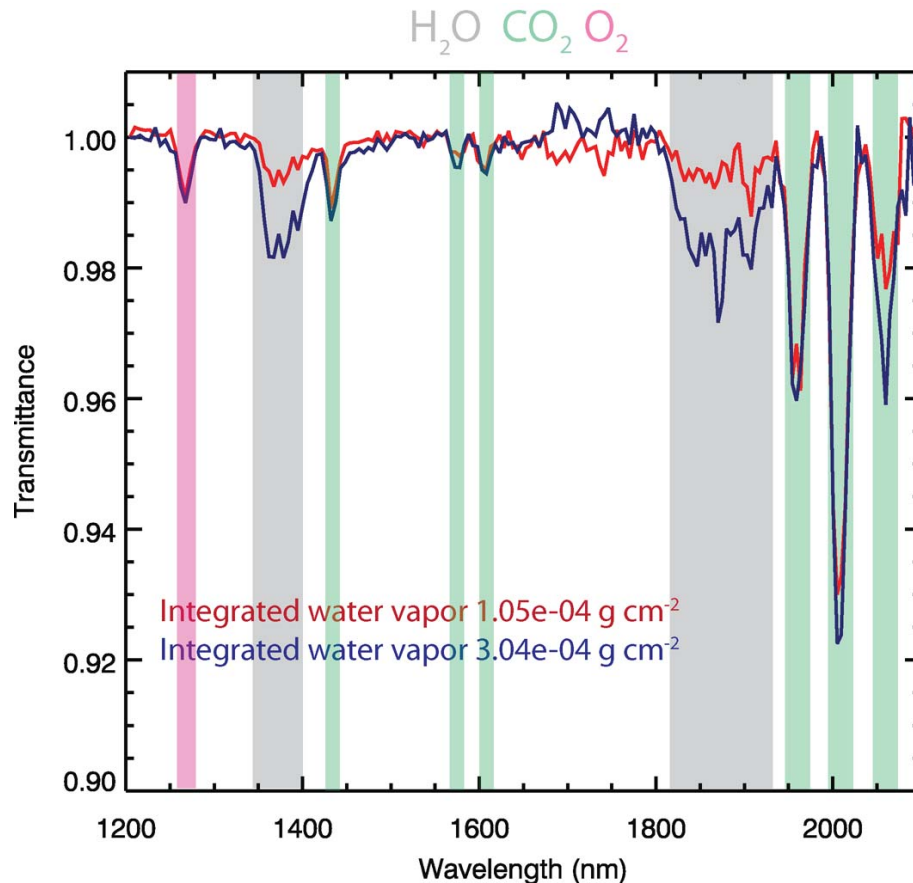


**Figure 4.** Transmittance spectra from the profiles shown in Fig. 2. Absorption band positions and widths are color coded: water vapor in gray, O<sub>2</sub> in magenta, and CO<sub>2</sub> in green. Integrated water vapor amounts in the figure indicate the corresponding water vapor column determined from the in situ measurements.

Title Page

Abstract

Introduction

Conclusions

References

Tables

Figures

◀

▶

◀

▶

Back

Close

Full Screen / Esc

Printer-friendly Version

Interactive Discussion



## UT and LS water vapor retrievals from the 1400 and 1900 nm water vapor bands

B. C. Kindel et al.

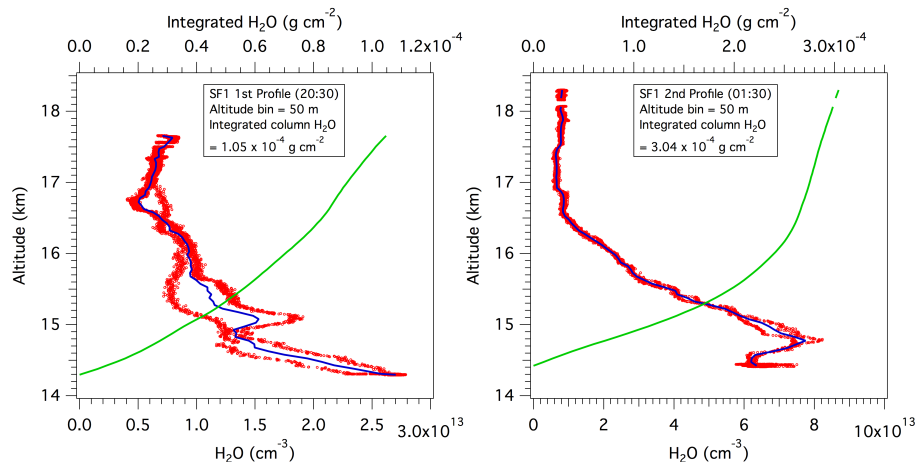


**Figure 5.** Water vapor number density profiles from the NOAA Water instrument. The red points correspond to the in situ water vapor number densities during the descent and ascent for the two profiles. The blue line is the mean of the ascent and descent number densities. The green line is the integrated water vapor amount (scale at the top of the plot). Note the large difference in the horizontal axis ranges and the integrated water vapor amounts between the two profiles.

[Title Page](#)
[Abstract](#)
[Introduction](#)
[Conclusions](#)
[References](#)
[Tables](#)
[Figures](#)
[Back](#)
[Close](#)
[Full Screen / Esc](#)
[Printer-friendly Version](#)
[Interactive Discussion](#)

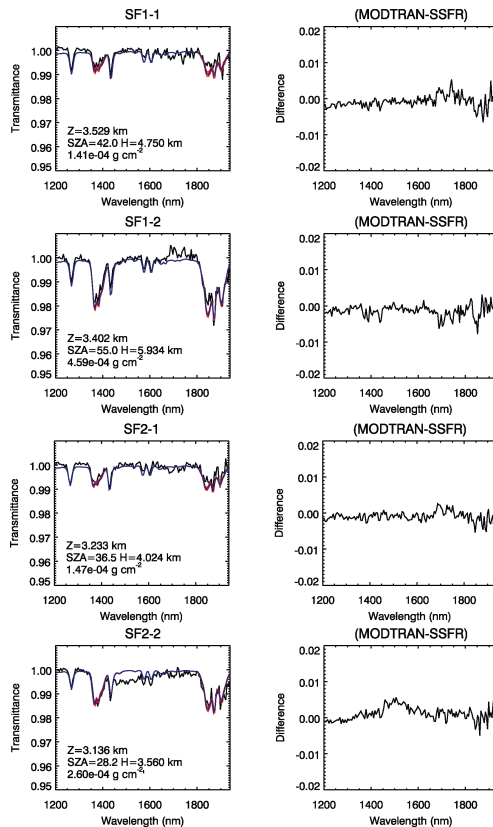


**Figure 6.** (left) Measured (black) and modeled (blue) transmittances for vertical profiles during the first and second ATTREX science flights are plotted. The red traces show plus and minus one standard deviation of the modeled transmittance. (right) Difference between the measured and modeled transmittances. The vertical profile distance  $Z$ , the solar zenith angle  $SZA$ , the absorption path length  $H$ , and the integrated water vapor amounts are given in the left hand plots.

UT and LS water vapor retrievals from the 1400 and 1900 nm water vapor bands

B. C. Kindel et al.

Title Page

Abstract Introduction

Conclusions References

Tables Figures

◀ ▶

◀ ▶

Back Close

Full Screen / Esc

Printer-friendly Version

Interactive Discussion



## UT and LS water vapor retrievals from the 1400 and 1900 nm water vapor bands

B. C. Kindel et al.

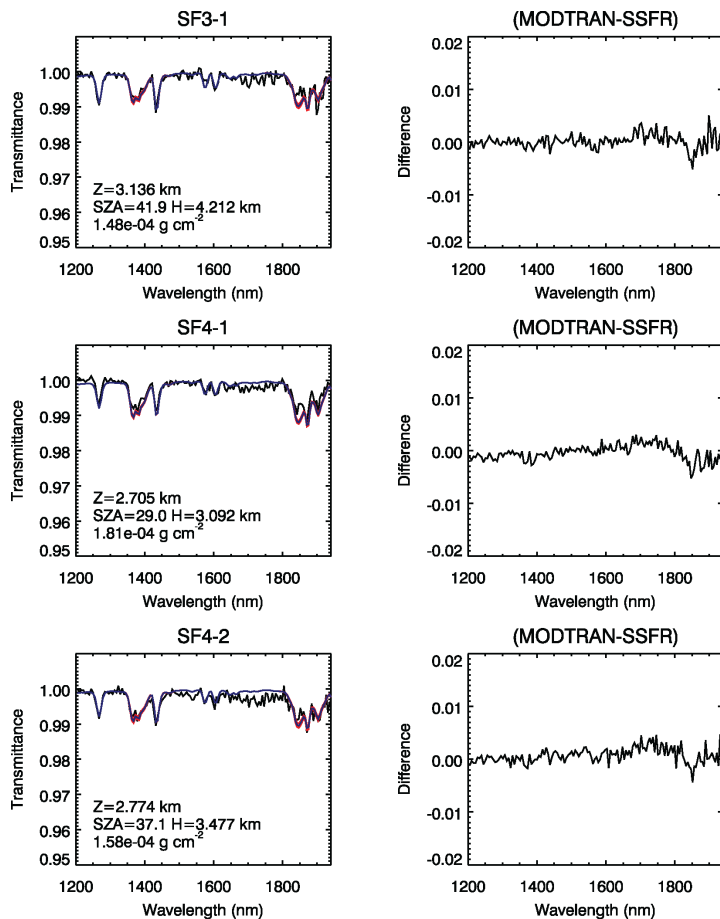


**Figure 7.** Same as Fig. 5 for profiles during the third and fourth ATTREX science flights.

Title Page

Abstract Introduction

Conclusions References

Tables Figures

◀ ▶

◀ ▶

Back Close

Full Screen / Esc

Printer-friendly Version

Interactive Discussion



## UT and LS water vapor retrievals from the 1400 and 1900 nm water vapor bands

B. C. Kindel et al.

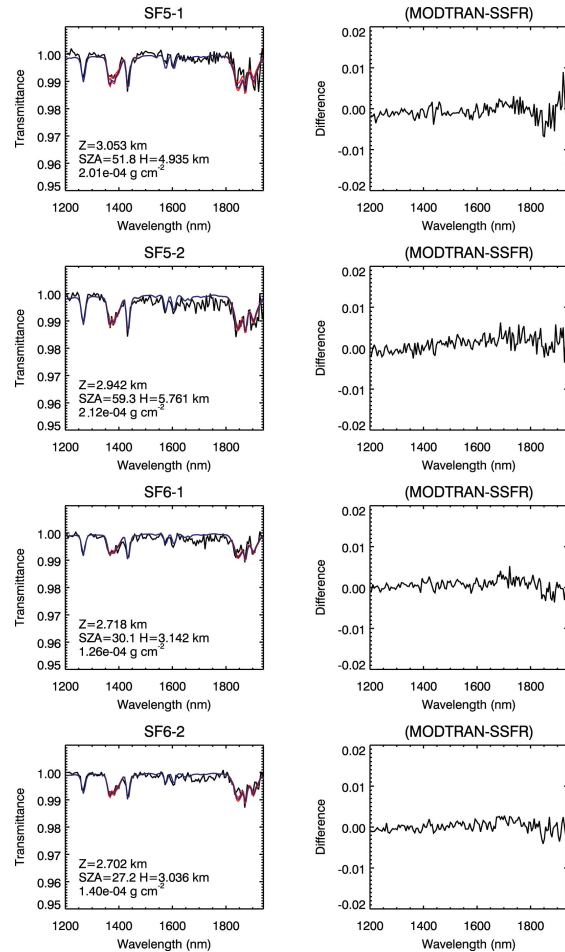


**Figure 8.** Same as Fig. 5 for profiles during the fifth and sixth ATTREX science flights.

Title Page

Abstract	Introduction
Conclusions	References
Tables	Figures

⏪ ⏩  
⏴ ⏵

Back Close

Full Screen / Esc

Printer-friendly Version

Interactive Discussion



**UT and LS water vapor retrievals from the 1400 and 1900 nm water vapor bands**

B. C. Kindel et al.

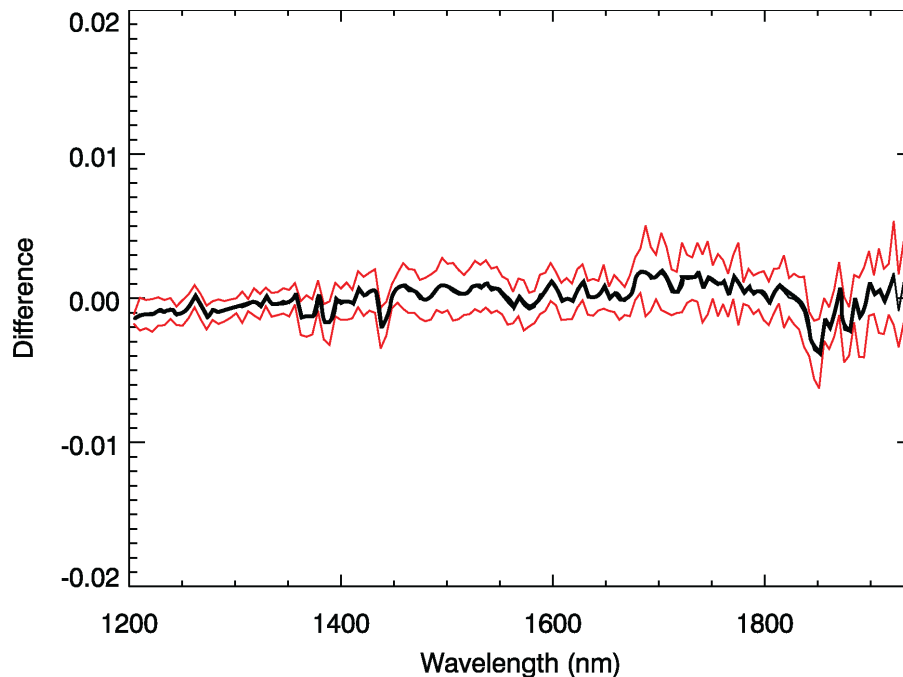


**Figure 9.** The mean (black) and standard deviation (red) difference (MODTRAN minus SSFR) spectra are plotted for the eleven profiles.

[Title Page](#)[Abstract](#)[Introduction](#)[Conclusions](#)[References](#)[Tables](#)[Figures](#)[◀](#)[▶](#)[◀](#)[▶](#)[Back](#)[Close](#)[Full Screen / Esc](#)[Printer-friendly Version](#)[Interactive Discussion](#)

## UT and LS water vapor retrievals from the 1400 and 1900 nm water vapor bands

B. C. Kindel et al.

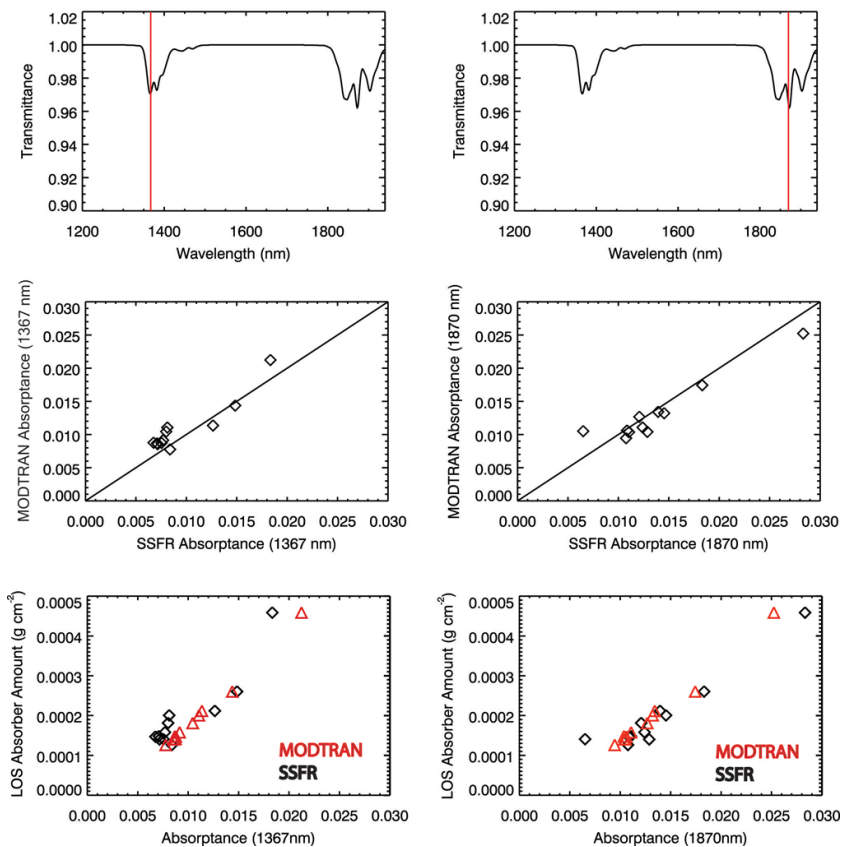


**Figure 10.** The top plots show modeled water vapor transmittance with the strongest part of each band indicated with a red vertical line. The middle panels show plots of SSFR measured vs. MODTRAN predicted absorptances at these wavelengths. The bottom panels show the measured and modeled absorptances plotted vs. the LOS integrated water vapor amount.

[Title Page](#)[Abstract](#)[Introduction](#)[Conclusions](#)[References](#)[Tables](#)[Figures](#)[◀](#)[▶](#)[◀](#)[▶](#)[Back](#)[Close](#)[Full Screen / Esc](#)[Printer-friendly Version](#)[Interactive Discussion](#)

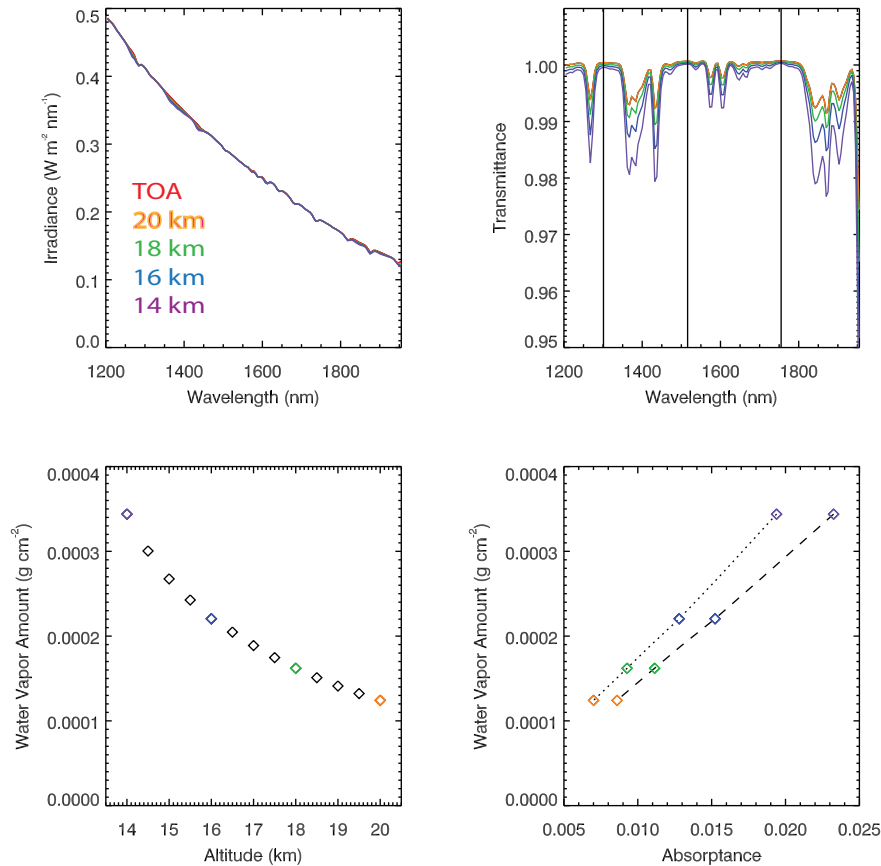


**Figure 11.** In the top left panel modeled irradiances are plotted. The top right panel shows the transmittance spectra for each altitude. In the bottom left panel integrated water vapor amount from the various altitudes to the TOA are plotted. In the bottom right panel the integrated water vapor amount is plotted as a function of absorbance at 1367 (dotted line) and 1870 nm (dashed line).